Deconvolution of the Potential and Time Dependence of Electrochemical Porous Semiconductor Formation

N. Quill,[1] C. O'Dwyer,[1] R. Lynch,[1,2] D. N. Buckley[1]

Materials and Surface Science Institute, University of Limerick, Ireland

[1] *Department of Physics, University of Limerick, Ireland*
[2] Present address: *Department of Materials Science, Institute for Surface Science and Corrosion (LKO), Friedrich-Alexander University of Erlangen-Nurmberg, Germany*

A layer of porous InP is grown beneath a thin dense surface layer when n-InP electrodes are anodized to sufficiently high potentials in aqueous KOH solutions. The shape of the linear sweep (LSV) or the cyclic voltammogram (CV) is dependent on carrier concentration. A technique is presented to deconvolute the effects of potential and time on a CV. The results obtained from this technique are used to explain the shape of the anodic current response and its relation to porous layer formation. The accuracy of the deconvolution technique is then tested by comparison to experimental results.

Introduction

The formation of porous structures during electrochemical etching of semiconductors under anodic bias has been the focus of considerable research efforts, due to the fundamental insight such studies reveal about semiconductor etching characteristics, and the potential applications of porous semiconductor structures (1-7). Although the bulk of this work has focused primarily on porous Si, a lot of attention has also been given to III-V compounds such as GaAs (8,9) and InP (10-12). There have been many models proposed (13-15) to account for the wide range of pore types, sizes and growth directions that have been observed. However, none of these models can predictably and accurately reproduce the variety of structures observed experimentally; such variations can be influenced by electrolyte type and concentration (16,17), substrate type (18), orientation (19) and doping density (20). The differences stem from the wide range of porous morphologies that are consistent with varied levels of dependence on potential, current and time, and on the relative reactivity of various crystal faces to their chemical environment. We previously reported nano-pore formation in n-InP electrodes anodized in >2 mol dm^{-3} KOH (17,21,22). These pores were shown to originate from pits etched in the surface and grow along the <111A> crystallographic directions ~(22), eventually forming a large porous domain beneath a thin (~40 nm) dense near-surface layer. The merging of the porous domains constitutes the formation of the entire porous layer.

To analyze the formation of these porous structures, linear sweep voltammetry (LSV) and cyclic voltammetry (CV) have been used. A technique to deconvolute the effects of potential and time on a CV has been developed and used to characterize the contribution/dependence of porous layer formation on potential and time during anodization.

Experimental

The working electrode consisted of polished (100)-oriented monocrystalline sulphur doped n-InP. An ohmic contact was made to the back of the InP sample and isolated electrically from the electrolyte by means of a suitable varnish. The electrode area was typically 0.1 cm^2. Two different InP wafers with different carrier concentrations, *n*, were used for two different series of experiments. InP anodes were used with carrier concentrations of $n = 5 – 5.6 \times 10^{18}$ cm^{-3} and a lower carrier concentration with $n = 2 – 4 \times 10^{18}$ cm^{-3}. The etch pit density of all samples used was less than 5×10^3 cm^{-2}. Anodization was carried out in aqueous 5 mol dm^{-3} KOH electrolytes. A conventional three-electrode cell configuration was used employing a platinum counter electrode and a saturated calomel reference electrode (SCE) to which all potentials were referenced. Prior to immersion in the electrolyte, the working electrode was dipped in an etchant (3:1:1 H_2SO_4:H_2O_2:H_2O) for 4 minutes and then rinsed in deionized water. All electrochemical experiments were carried out in the absence of light at room temperature.

A CH Instruments Model 650A Electrochemical Workstation was employed for cell parameter control and for data acquisition. Cleaved {011} cross-sections were examined using a Hitachi S-4800 field emission scanning electron microscope (SEM) operating at 5 kV.

Results and Discussion

A typical LSV for n-InP (carrier concentration = 5 - 5.6×10^{18} cm^{-3}) at 2.5 mV s^{-1} in 5 mol dm^{-3} KOH is shown in Figure 1. Initially, the increase in potential corresponds to a small increase in current until a potential E_{pit} is reached; E_{pit} is the potential at which the first etch pits appear on the InP surface (23), as shown in the inset micrograph, Fig. 1a.

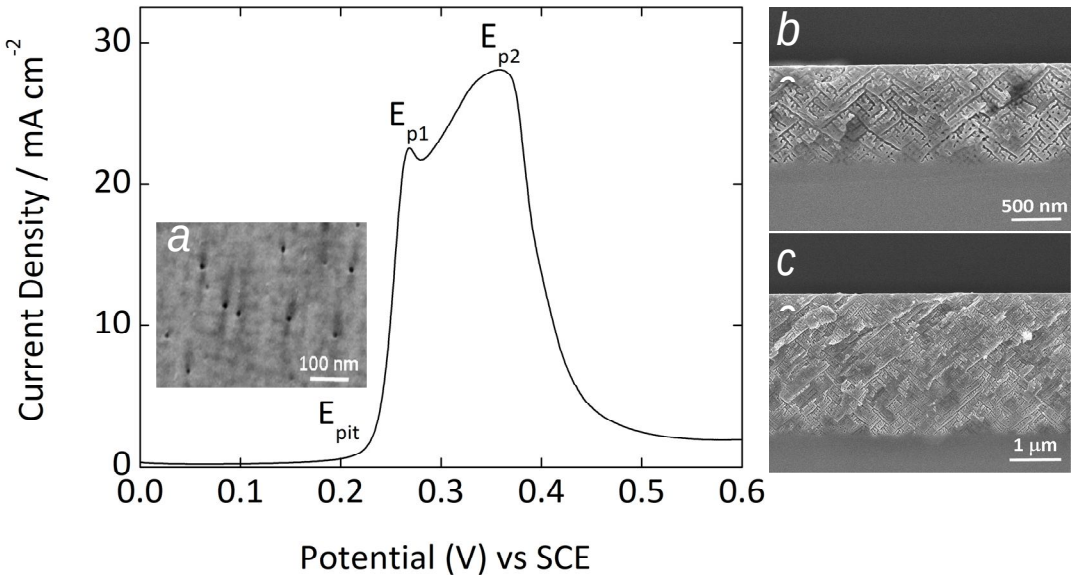

Fig. 1 Linear sweep voltammogram of an n-type InP electrode ($n = 5 – 5.6 \times 10^{18}$ cm^{-3}) in 5 mol dm^{-3} KOH at a scan rate of 2.5 mV s^{-1}. The potential was swept from 0.0 V to 0.6 V (SCE). Labelled on the plot are the pitting potential E_{pit} (0.22 V), the potential of the first current peak E_{p1} (0.27 V) and the potential of the second current peak E_{p2} (0.36 V). The SEM images were acquired after anodization to (a) E_{pit} (b) E_{p1} and (c) E_{p2}.

Deconvolution of the cyclic voltammetric response

At potentials greater than E_{pit}, the current begins to increase at a much faster rate; this current exhibits two peaks at E_{p1} and E_{p2}. In relation to the characteristics of porous layer growth observed in these samples, these current peaks correspond to merging of porous domains by growth in lateral and vertical directions, and to continued vertical growth (deepening) of the complete porous layer. This can be observed in the micrographs shown in Figs 1b and 1c. To determine to what extent the increase in current is caused by increasing potential, compared to what would be observed under potentiostatic conditions, a technique to deconvolute the effects (or contribution) of potential and time is presented below.

As the measured current I in a cyclic voltammogram (CV) is a function of both potential E and time t, we can write

$$I = I(E,t) \tag{1}$$

Therefore

$$dI = \left(\frac{\partial I}{\partial t}\right)_E dt + \left(\frac{\partial I}{\partial E}\right)_t dE \tag{2}$$

If v is the scan rate then $E = vt$ and

$$dI = \left(\frac{\partial I}{\partial t}\right)_E dt + v\left(\frac{\partial I}{\partial E}\right)_t dt \tag{3}$$

Also,

$$dI = \frac{1}{v}\left(\frac{\partial I}{\partial t}\right)_E dE + \left(\frac{\partial I}{\partial E}\right)_t dE \tag{4}$$

Thus, at any potential E_{exp} on a cyclic voltammogram, the slope of the forward and reverse curves respectively are

$$\left(\frac{dI}{dE}\right)_{FWD,E_{exp}} = \frac{1}{v}\left(\frac{\partial I}{\partial t}\right)_E + \left(\frac{\partial I}{\partial E}\right)_t \tag{5}$$

and

$$\left(\frac{dI}{dE}\right)_{REV,E_{exp}} = -\frac{1}{v}\left(\frac{\partial I}{\partial t}\right)_E + \left(\frac{\partial I}{\partial E}\right)_t \tag{6}$$

Although the functional relationship in Eqn. 1 is not necessarily the same for the forward and reverse curves, it is assumed that it is instantaneously the same at the point of potential reversal E_u. Thus it follows from Eqns 5 and 6 that

$$\left(\frac{\partial I}{\partial E}\right)_t = \frac{\left(\frac{dI}{dE}\right)_{FWD,E_u} + \left(\frac{dI}{dE}\right)_{REV,E_u}}{2} = \frac{m_f + m_r}{2} \tag{7}$$

and

$$\left(\frac{\partial I}{\partial t}\right)_E = \frac{\nu\left\{\left(\frac{dI}{dE}\right)_{FWD,E_u} - \left(\frac{dI}{dE}\right)_{REV,E_u}\right\}}{2} = \frac{\nu\left(m_f - m_r\right)}{2} \qquad (8)$$

where m_f and m_r are the forward and reverse slopes at E_u. From Eqns 7 and 8 the effect of potential and time on a cyclic voltammogram at the point of potential reversal can be calculated simply by measuring the slopes of the current response from CVs in the forward and reverse directions.

A series of cyclic voltammograms were obtained for the higher carrier concentration samples, in which the potential was scanned from 0 V to more anodic values of the upper potential E_u over a range of scan rates (0.625 mV s^{-1} to 10 mV s^{-1}) in 5 mol dm^{-3} KOH. Typical cyclic voltammograms are shown in Fig. 2 at a single potential scan rate, where E_u is less than the first peak (E_{p1} from Fig. 1) in the LSV. It can be seen that when the potential sweep is reversed, the current increases initially until it reaches a peak, after which the current decreases non-linearly with decreasing potential.

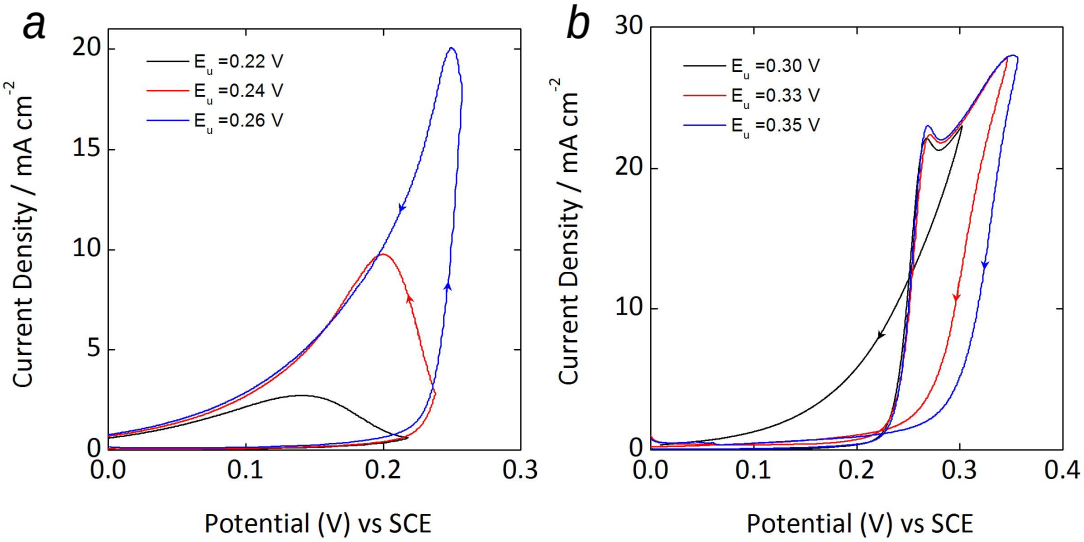

Fig. 2 Cyclic voltammograms of n-type InP electrodes (n = 5 – 5.6 × 10^{18} cm^{-3}) in 5 mol dm^{-3} KOH at a scan rate of 2.5 mV s^{-1} with (a) E_u = 0.22 V, 0.24V, and 0.26 V (SCE) and (b) E_u = 0.3 V, 0.35 V and 0.36 V (SCE).

In Fig. 2b, CVs of InP anodes with $E_u > E_{p1}$ are shown. On the reverse scan, the current densities are lower than the corresponding current densities on the forward scan and continue to decrease as the potential is decreased. Of note, we observe negligible hysteresis in CVs where $E_u = E_{p1}$, *i.e.* the reverse scan current overlays the forward scan current values.

From CVs with a range of upper potentials E_u, the slopes of the forward and reverse curves, m_f and m_r, were estimated. The resulting values are plotted in Fig. 3. The slope of the forward curve has the expected dependence for the derivative of the peaks in the cyclic voltammogram (a corresponding LSV is superimposed on Fig. 3 for comparison). The reverse slope behaves in roughly the opposite way. From the data in Fig. 3, $(\partial I/\partial E)_t$ and $(\partial I/\partial t)_E$ were estimated according to Eqns 7 and 8, and the values obtained were plotted against upper potential E_u to obtain the plot in Fig. 4.

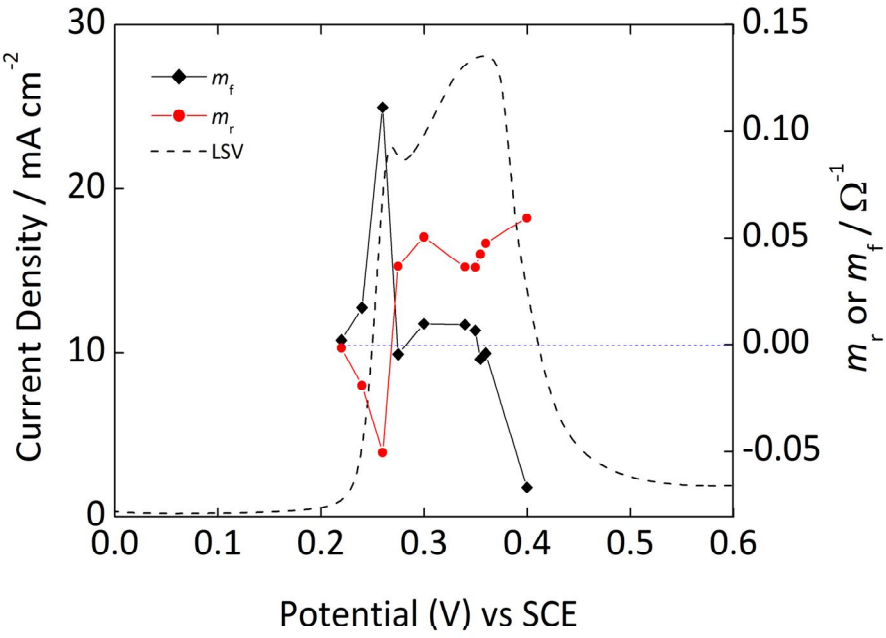

Fig. 3 Potential dependence of the slopes of the forward and reverse curves, m_f and m_r, at the upper potential limit E_u for a series of cyclic voltammograms of n-InP electrodes (n = 5 – 5.6 × 10^{18} cm^{-3}) in 5 mol dm^{-3} KOH at a scan rate of 2.5 mV s^{-1}. The corresponding LSV is also shown for comparison.

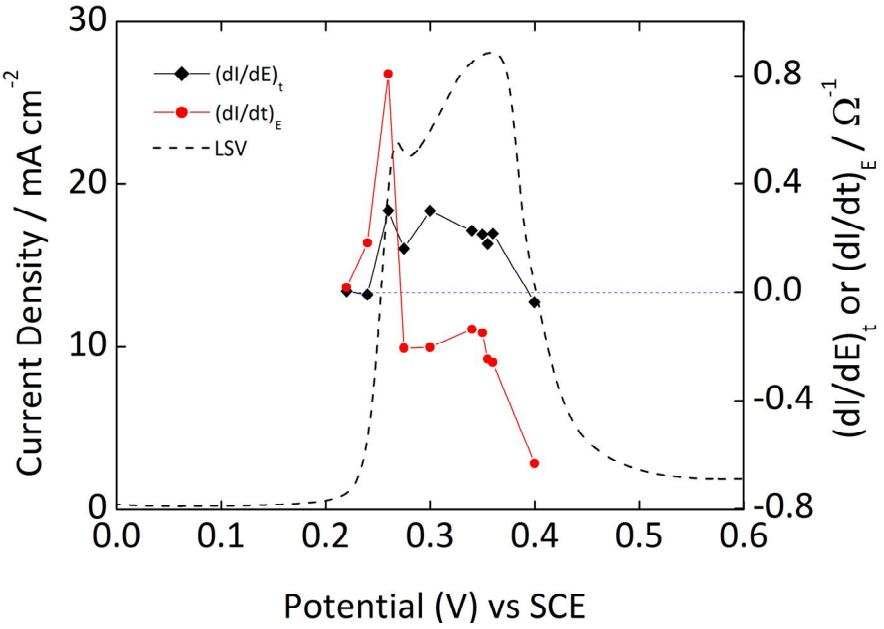

Fig. 4 Variation of $(\partial I/\partial E)_t$ and $(\partial I/\partial t)_E$ at the upper potential limit E_u, derived from the data in Fig. 3 for CVs of InP electrodes (n = 5 – 5.6 × 10^{18} cm^{-3}) in 5 mol dm^{-3} KOH at a scan rate of 2.5 mV s^{-1}. The corresponding LSV is shown for comparison. The values for $(\partial I/\partial t)_E$ as calculated by Eqn. 8, were scaled by a multiplicative factor of 400 s V^{-1} (*i.e.* the inverse of the scan rate).

It can be seen that at potentials less than 0.22 V (E_{pit}), both quantities are essentially null since the current flowing at that potential is very small (~1 mA cm^{-2}). However, $(\partial I/\partial t)_E$ rises sharply after E_{pit} and stays much larger than $(\partial I/\partial E)_t$ until the first peak, $E_{p1,}$ is reached. Then, between E_{p1} and the second peak, $E_{p2,}$ it is $(\partial I/\partial E)_t$ that is dominant. Finally, as the current begins to decrease, $(\partial I/\partial E)_t$ becomes approximately 0 and $(\partial I/\partial t)_E$ dominates once again.

These experiments were repeated for n-InP samples with a carrier concentration in the range 2 – 4 × 10^{18} cm^{-3}. The LSV of the lower carrier concentration anode is shown as a dashed line in Fig. 5a. The most obvious difference with respect to Fig. 2 is that there is now only one current peak. It is also noted that this peak occurs at a higher potential (E_p = 0.48 V (SCE)) than the peaks in Fig. 2. The corresponding CVs with E_u less than the peak potential are shown for the lower carrier concentration sample in Fig. 5a. It can be seen that upon reversing the potential sweep, the current continues to increase and eventually reaches a peak, before decreasing with reducing applied potential. Figure 5b shows corresponding CVs with E_u greater than the peak potential. The current density is routinely observed to decrease for the entire reverse sweep. Clearly the behaviour of the lower doped electrodes around the peak potential is the same as the behaviour of the more highly doped electrodes at potentials close to E_{p1}.

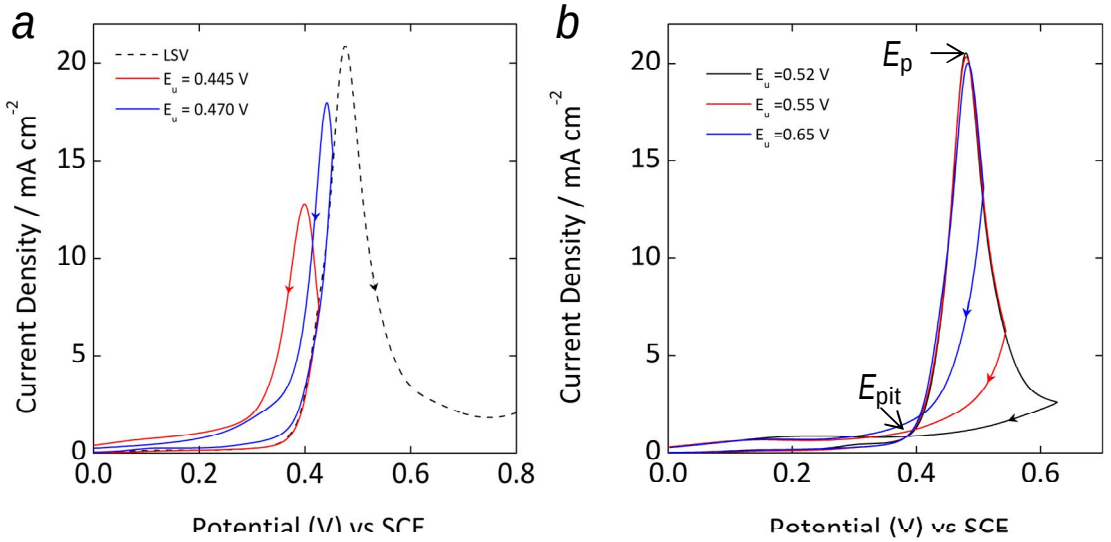

Fig. 5 Cyclic voltammograms of InP electrodes (n = 2 – 4 × 10^{18} cm^{-3}) in 5 mol dm^{-3} KOH at a scan rate of 2.5 mV s^{-1} with (a) E_u = 0.445 V and 0.47 V (SCE) and (b) E_u = 0.52 V, 0.55 V and 0.65 V. The linear potential sweep from 0.0 V to 0.8 V at 2.5 mV s^{-1} is also shown (dashed line in (a)).

As before, the slopes of the forward and reverse curves, m_f and m_r, were estimated from cyclic voltammograms (of the lower carrier concentration InP) to a range of upper potentials, and the resulting values are plotted in Fig. 6. The deconvolution technique was applied to this data and the results are plotted in Fig. 7.

It can be seen from Fig. 7 that the changing potential minimal effect on the current flow for the InP samples of lower carrier concentration. The increase in current (and also its decrease) is observed to occur under potentiostatic conditions (where the potential is stepped to values in the range E and this has been verified by experiment (21).

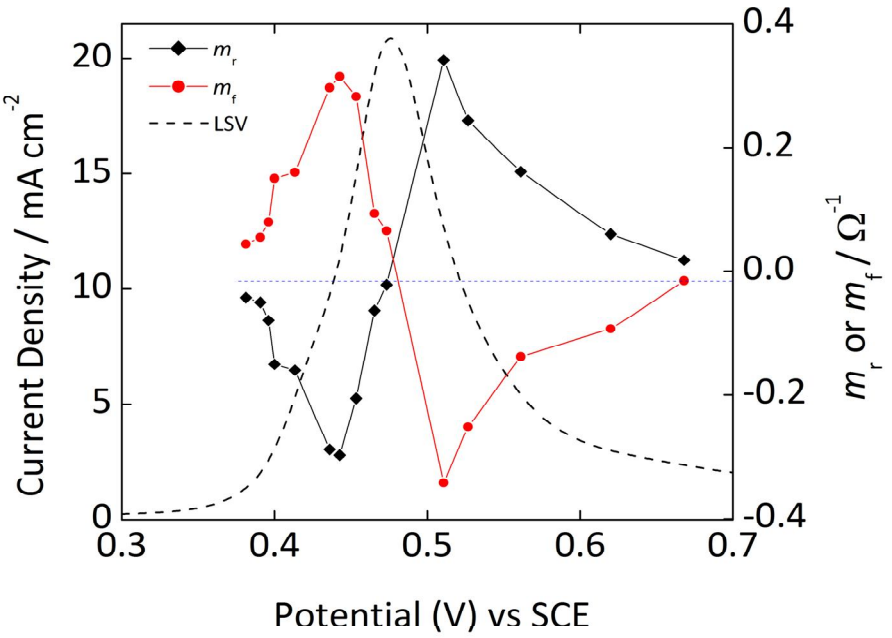

Fig. 6 Potential dependence of the slopes of the forward and reverse curves, m_f and m_r, at the upper potential limit E_u for a series of cyclic voltammograms of n-InP electrodes (n = 2 – 4 × 10^{18} cm^{-3}) in 5 mol dm^{-3} KOH at a scan rate of 2.5 mV s^{-1}. The corresponding LSV is shown for comparison.

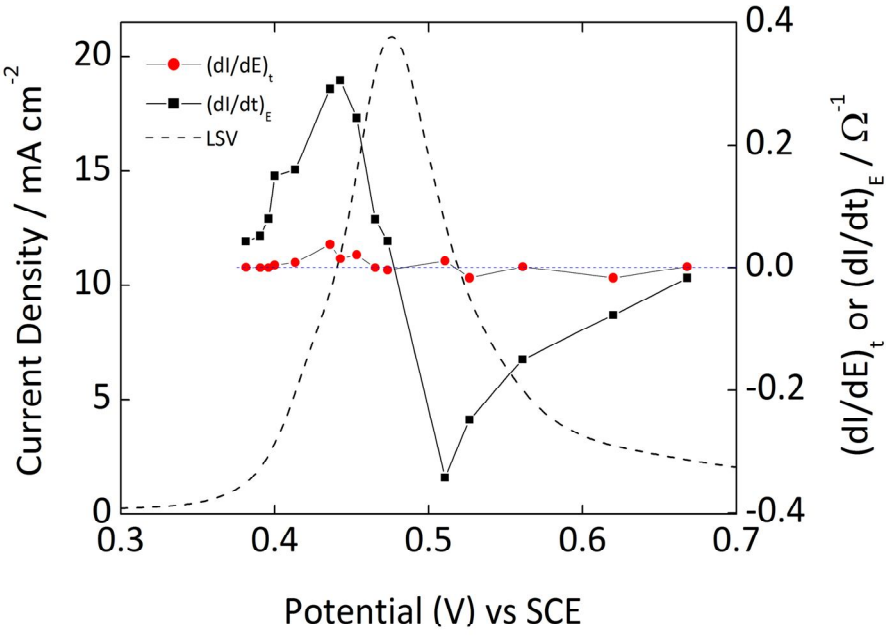

Fig. 7 Potential dependence of $(\partial I/\partial E)_t$ and $(\partial I/\partial t)_E$ at the upper potential limit E_u, derived from the data in Fig. 6 for cyclic voltammograms of InP electrodes (carrier concentration = 2 – 4 × 10^{18} cm^{-3}) in 5 mol dm^{-3} KOH at a scan rate of 2.5 mV s^{-1}. The values for $(\partial I/\partial t)_E$ as calculated by Eqn 8, were scaled by a multiplicative factor of 400 s V^{-1} (*i.e.* the inverse of the scan rate). The corresponding LSV is shown for comparison.

The principal difference between the anodic behaviour of the two InP anodes is that the higher carrier concentration sample reaches its peak in current at a much lower potential. At potentials greater than E_{p1}, the current continues to increase linearly until a second peak is reached. This potential controlled region is completely absent from the deconvoluted curve of InP samples doped at $n = 2 - 4 \times 10^{18}$ cm^{-3}. Dedicated AFM and SEM observations have shown that both the solitary peak in the low concentration sample (*c.f.* Fig. 5a), and E_{p1} in the higher concentration sample (*c.f.* Fig. 1), correspond to the merging of porous domains to form one continuous porous layer beneath the surface (23).

Relating the deconvolution technique to porous layer growth

These results can be understood in the framework of the following model for the relation between the shape of the LSV and the characteristics of porous layer growth. At potentials less than E_{pit}, almost no current flows through the electrode because of the space charge double layers that are present at the interface between electrode and electrolyte; no etching would formally occur in the case of complete carrier depletion in the InP. As the potential is increased past E_{pit}, carriers can gain enough energy to tunnel through the space charge layer resulting in the initiation of etching at the surface (21). From this point on the current begins to increase rapidly. This is due to more and more pits forming in the surface as the potential is increased and the sub-surface propagation of etching pore tips within the porous domains. This leads to an increased number of current paths and consequently an increased current density. Deconvolution of the CVs associated with porous layer growth suggests that the increase is much more significant than can be accounted for by the increasing potential alone.

The onset of the first current peak corresponds to the merging of the porous domains into a single porous layer, as shown in Fig. 1. As the potential is increased further, the current density increase cannot be accounted for by just an increase in the area it flows through. This corresponds to a limit in the number of new/existing pore formation/growth after complete domain merging. Therefore any increase in current density must be directly due to processes driven by an increase in applied potential. Even though no new domains can form, the current can still cause existing domains to grow in the vertical direction. This is what is observed after E_{p1} in the higher carrier concentration sample. The increase in depth of the fully formed porous layer occurs as the current density increases linearly with increasing potential. Only a single peak is observed for the lower carrier concentration samples under identical conditions. In addition, porous layers formed in such samples do not grow to the same depth after domain merging (~1 μm for the low concentration sample and ~3 μm for the high concentration sample). Similar behaviour is observed in the higher carrier concentration electrode after the second current peak, E_{p2}.

To assess the accuracy and applicability of the deconvolution technique to porous layer growth, a series of experiments were performed (using the higher carrier concentration samples) in which the potential was scanned from 0 V to different values of E_u. The potential E_u was then held constant in order to observe the effect of time on the electrochemical process. The slope of the current-time curve was measured to verify that the value of $(\partial I/\partial t)_E$ given by the deconvolution technique agrees with experimental observation and the results are given in Fig. 8. We observe good agreement in the data in Fig. 8, showing that the technique can produce quantitative information on independent potential and time contributions to the growth of the porous layer.

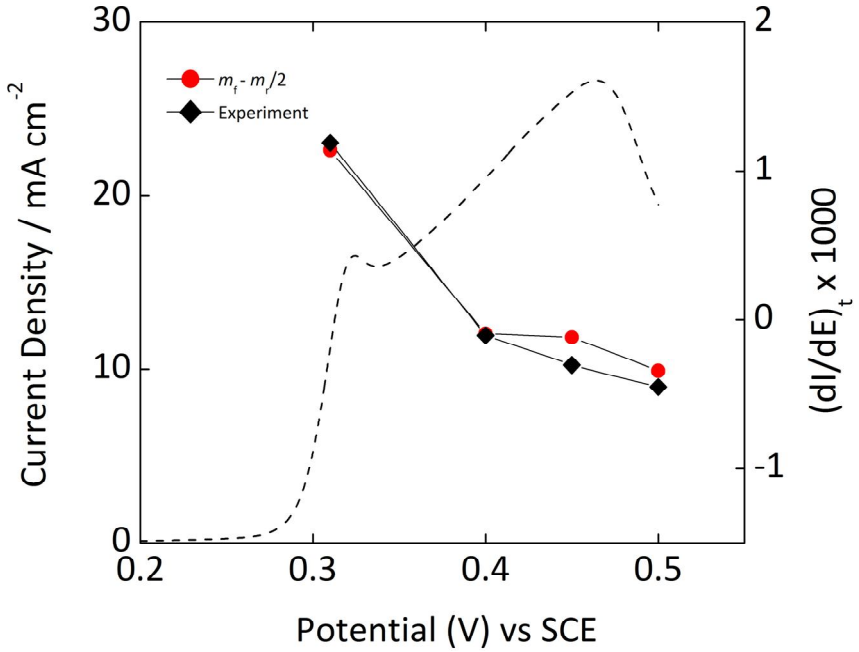

Fig. 8 Plot of the rate of change of current with respect to time at constant potential $(\partial I/\partial t)_E$ for InP anodes ($n = 5 - 5.6 \times 10^{18}$ cm^{-3}) anodized in 5 mol dm^{-3} KOH as measured by experiment and calculated by the deconvolution technique. The corresponding LSV is superimposed for comparison.

Conclusions

A technique to deconvolute the effects of potential and time on linear and cyclic sweep voltammograms was developed and used to explain the shape of the anodic response of n-InP in 5 mol dm^{-3} KOH. This technique analyzes the instantaneous value of the rate of change of current with respect to time and potential by extracting the slopes of the current profile acquired during porous layer formation. Characteristic voltammograms are observed for n-InP anodes with different carrier concentrations. For InP electrodes with $n = 5 - 5.6 \times 10^{18}$ cm^{-3}, the voltammetric response showed two distinct current peaks on the forward potential sweep; the first current peak was shown to be caused by the merging of porous domains (growing both vertically and laterally) into a continuous porous layer. In this potential region, the porous layer growth is predominatly a function of time, i.e. the porous layer would continue to grow if the potential was swept to, and held, at values in the range $E_{pit} - E_{p1}$. The 'ohmic' increase in current after the first peak was shown to be due to the vertical growth of the fully formed porous layer.

The deconvolution technique was shown to be valid at different carrier concentrations and potential sweep rates. InP anodes with $n = 2 - 4 \times 10^{18}$ cm^{-3}, only exhibited a single current peak on the forward sweep, but equally amenable to deconvolution using this technique. The deconvoluted values for $(\partial I/\partial t)_E$ and $(\partial I/\partial E)_t$ agree well with the experimental values obtainable for these quantities, showing the technique to be both qualitatively and quantitatively accurate in relating the cyclic voltammogram to the resulting porous layer formation.

References

(1) L.T. Canham, *Appl. Phys. Lett.*, **57**, 1046 (1990).
(2) H. Föll, *Appl. Phys. A*, **53**, 8 (1991).
(3) T. Holec, T. Chvojka, I. Jelínek, J. Jindřich, I. Němec, I. Pelant, J. Valenta and J. Dian, *Mater. Sci. Eng. C*, **19**, 251 (2002).
(4) R.J. Martín-Palma, J.M. Martínez-Duart, L. Li and R.A. Levy, *Mater. Sci. Eng. C*, **19**, 359 (2002).
(5) A. Matoussi, T. Boufaden, A. Missaoui, S. Guermazi, B. Bessaïs, Y. Mlik and B. El Jani, *Microelectronics Journal*, **32**, 995 (2001).
(6) A. Jain, S. Rogojevic, S. Ponoth, N. Agarwal, I. Matthew, W.N. Gill, P. Persans, M. Tomozawa, J.L. Plawsky and E. Simonyi, *Thin Solid Films*, **398**, 513 (2001).
(7) N.E. Chayen, E. Saridakis, R. El-Bahar, Y. Nemirovsky, *J. Molec. Biol.*, **312**, 591 (2001).
(8) S. Langa, J. Carstensen, M. Christophersen, H. Föll, and I.M. Tiginyanu, *Appl. Phys. Lett.*, **78**, 1074 (2001).
(9) G. Oskam, A. Natarajan, P.C. Searson and F.M. Ross, *Appl. Surf. Sci.*, **119,** 160 (1997).
(10) S. Langa, J. Carstensen, I.M. Tiginyanu, M. Christophersen and H. Föll, *Electrochem. Solid-State Lett.*, **4,** G50 (2001).
(11) S. Langa, I.M. Tiginyanu, J. Carstensen, M. Christophersen and H. Föll, *Electrochem. Solid-State Lett.* **3**, 514 (2000).
(12) R.L. Smith and S.D. Collins, *J. Appl. Phys.*, **71**, 8 (1992).
(13) H. Föll et al, *Phys. Stat. Sol. (a)*, **182,** 7 (2000).
(14) T. Unagami, *J. Electrochem. Soc.*, **127**, 476 (1980).
(15) V. Lehmann and U. Gösele, *Appl. Phys Lett.* **58**, 856 (1991).
(16) P. Schmuki, J. Fraser, C.M. Vitus, M.J. Graham, H.S. Isaacs, *J. Electrochem. Soc.*, **143**, 3316 (1996).
(17) R. Lynch, C. O'Dwyer, D.N. Buckley, D. Sutton and S.B. Newcomb, *ECS Trans.*, **2,** 131 (2006).
(18) M. Christopherson, J. Carstensen, A. Feuerhake and H. Föll, *Mater. Sci. Eng. B*, **69**, 70, 194 (2000).
(19) S. Rönnebeck, J. Carstensen, S. Ottow and H. Föll, *Electrochem. Solid-State Lett.*, **2**, 126 (1999).
(20) P. Schmuki, L.E. Erickson, D.J. Lockwood, J.W. Fraser, G. Champion, H.J. Labbé, *Appl. Phys. Lett.*, **72,** 1039 (1998).
(21) C. O'Dwyer, D.N. Buckley, M. Serantoni, D. Sutton and S.B. Newcomb, in *Proceedings of the State-of-the-Art Program on Compound Semiconductors XXXIX*, R.F. Kopf, D.N. Buckley, F. Ren, C. Monier, K. Shiojima, A.G. Baca, H.M. Ng, T.D. Moustakas, S.J. Pearton, Editors, **PV 2003-11**, p. 136, The Electrochemical Society, Proceedings Series, Pennington, NJ (2003)
(22) R. Lynch, C. O'Dwyer, D. Sutton, S.B. Newcomb and D.N. Buckley, *ECS Trans.*, **6**, 355 (2007).
(23) C. O'Dwyer, D.N. Buckley, D. Sutton, M. Serantoni and S.B. Newcomb, *J. Electrochem. Soc.*, **154**, H78 (2007).